

Filled and glycosylated carbon nanotubes for *in vivo* radioemitter localization and imaging

Sung You Hong¹, Gerard Tobias^{2,3*}, Khuloud T. Al-Jamal⁴, Belén Ballesteros^{2,5}, Hanene Ali-Boucetta⁴, Sergio Lozano-Perez⁶, Peter D. Nellist⁶, Robert B. Sim⁷, Ciara Finucane⁸, Stephen J. Mather⁸, Malcolm L. H. Green², Kostas Kostarelos^{4*} and Benjamin G. Davis^{1*}

Functionalization of nanomaterials for precise biomedical function is an emerging trend in nanotechnology¹. Carbon nanotubes are attractive as multifunctional carrier systems because payload can be encapsulated in internal space whilst outer surfaces can be chemically modified². Yet, despite potential as drug delivery systems^{3,4} and radiotracers^{5–8}, such filled-and-functionalized carbon nanotubes have not been previously investigated *in vivo*. Here we report covalent functionalization of radionuclide-filled single-walled carbon nanotubes and their use as radioprobes. Metal halides, including Na¹²⁵I, were sealed inside single-walled carbon nanotubes to create high-density radioemitting crystals⁹ and then surfaces of these filled-sealed nanotubes were covalently modified with biantennary carbohydrates, improving dispersibility and biocompatibility¹⁰. Intravenous administration of Na¹²⁵I-filled glyco-single-walled carbon nanotubes in mice was tracked *in vivo* using single-photon emission computed tomography. Specific tissue accumulation (here lung) coupled with high *in vivo* stability prevented leakage of radionuclide to high-affinity organs (thyroid/stomach) or excretion, and resulted in ultrasensitive imaging and delivery of unprecedented radiodose density. Nanoencapsulation of iodide within single-walled carbon nanotubes enabled its biodistribution to be completely redirected from tissue with innate affinity (thyroid) to lung. Surface functionalization of ¹²⁵I-filled single-walled carbon nanotubes offers versatility towards modulation of biodistribution of these radioemitting crystals in a manner determined by the capsule that delivers them. We envisage that organ-specific therapeutics and diagnostics can be developed on the basis of the nanocapsule model described here.

Single-walled carbon nanotubes (SWNTs) can be filled with a large variety of compounds, ranging from organic molecules^{11,12} to inorganic materials⁹. Other carbon materials, such as the endohedral fullerenes, can also be filled with smaller numbers of (for example, paramagnetic^{13,14} or radioemitting^{13–15}) atoms, although, similarly, they have not yet been realized as agents *in vivo*¹⁴. When nanotube filling is carried out at high temperature, the ends of the SWNTs spontaneously close on cooling, resulting in closed-ended filled SWNT capsules¹⁶. The excess of material external to the SWNTs may then be dissolved away by choice

of a suitable solvent. The contents of these filled and sealed SWNTs pack in a dense manner, leading to interesting and unusual crystalline phases⁹. Here, CuBr and NaI salts were encapsulated inside steam-purified-and-shortened¹⁷ SWNTs by molten-phase capillary wetting, resulting in nanocapsules containing the metal halides free of external material. The successful encapsulation of the metal halides in the SWNTs was confirmed by high-resolution transmission electron microscopy and scanning transmission electron microscopy (STEM).

So far, functionalization of the surface of carbon nanotubes has often been based on the attachment of building blocks to carboxylic acid groups, which can be formed by oxidation by nitric acid treatment¹⁸. Other approaches^{19–21} have demonstrated the potential of non-covalent decoration of nanotubes, enabling, for example, interaction with proteins and cells. However, nitric acid treatment of our filled SWNTs to introduce carboxylic acid groups on the sample resulted in the complete loss of the encapsulated metal halides (Supplementary Information), because during the oxidation process the ends of the sealed nanotubes are re-opened²². As an alternative, milder strategy for the primary covalent functionalization of SWNTs, we chose the azomethine ylid 1,3-dipolar cycloaddition reaction previously reported^{3,5}. This reaction does not require the use of metal catalyst and preserved the tubular structure and the closed ends of the nanotubes during treatment, avoiding both external metal contamination or the release of the filled material. For first evaluations using electron microscopy imaging, the 2,3,5-triiodophenyl motif was introduced to the functional groups as a tagging agent. Since *Z*-contrast STEM imaging is strongly dependent on the atomic number *Z* of the observed atom²³, rational design of organic molecules containing heavy-element tags, such as iodine, enables their atomic-scale detection²⁴. As an initial approach, SWNTs were filled with CuBr (Supplementary Fig. S1). After removal of the external, non-encapsulated, CuBr, the nanocapsules were then functionalized via 1,3-dipolar cycloaddition to show different elements in their interior and on their surface that could be observed by various methods. The reaction mixture of NBoc-amino acid **1**, 2,3,5-triiodobenzaldehyde **2** and CuBr@SWNTs was refluxed in *N,N*-dimethylformamide to create first examples of filled-sealed-functionalized nanocapsular SWNTs, f-CuBr@SWNTs (Fig. 1).

¹Department of Chemistry, University of Oxford, Chemistry Research Laboratory, Mansfield Road, Oxford OX1 3TA, UK, ²Department of Chemistry, University of Oxford, Inorganic Chemistry Laboratory, South Parks Road, Oxford OX1 3QR, UK, ³Institut de Ciència de Materials de Barcelona (ICMAB-CSIC), Campus UAB, 08193 Bellaterra, Barcelona, Spain, ⁴Nanomedicine Lab, Centre for Drug Delivery Research, The School of Pharmacy, University of London, London WC1N 1AX, UK, ⁵Centre d'Investigació en Nanociència i Nanotecnologia (ICN-CSIC), Campus UAB, 08193 Bellaterra, Barcelona, Spain, ⁶Department of Materials, University of Oxford, Parks Road, Oxford OX1 3PH, UK, ⁷Department of Pharmacology, University of Oxford, Mansfield Road, Oxford OX1 3QT, UK, ⁸Department of Nuclear Medicine, St Bartholomew's Hospital, London EC1A 7BE, UK.

*e-mail: gerard.tobias@icmab.es; kostas.kostarelos@pharmacy.ac.uk; ben.davis@chem.ox.ac.uk.

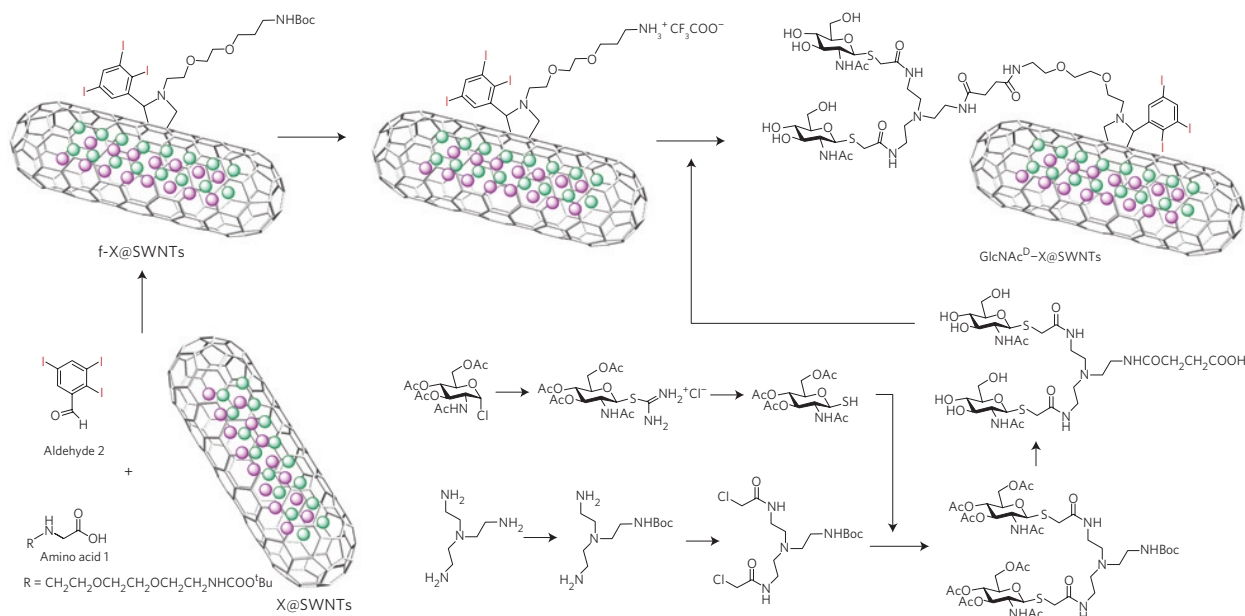


Figure 1 | Preparation of the construct. Synthesis of GlcNAc^D and GlcNAc^D-X@SWNTs (X = CuBr, NaI or Na¹²⁵I) (see Supplementary Information for details).

Thermogravimetric analysis revealed a 23.9 wt% filling yield²⁵ (calculated 3.11×10^{-19} g/SWNT) of CuBr and a 0.17 mmol g⁻¹ loading of organic functional groups onto the surface of the SWNTs (Supplementary Fig. S2).

Samples of filled SWNTs were examined before and after functionalization by Z-contrast STEM (Fig. 2). Although the Z-contrast STEM images of CuBr@SWNTs revealed one-dimensional crystals along the SWNT capillary, f-CuBr@SWNTs showed the simultaneous presence of CuBr inside the SWNTs as well as iodine along the SWNT walls. Intensity profiles on the Z-contrast images provided further evidence for functionalization of the filled SWNTs, presenting a 106% increase from the vacuum background signal for f-CuBr@SWNTs compared with a 56% increase for the filled-only CuBr@SWNT sample (brightness and contrast settings adjusted to produce similar background intensities in the vacuum for both analysed areas (around 9,000 counts)). Energy-dispersive X-ray spectroscopy (EDS) (Fig. 2f) corroborated the presence of the three additional elements Cu, Br and I that constitute the f-CuBr@SWNTs. Elemental EDS mapping in STEM mode (Supplementary Fig. S5) also confirmed concentration of Cu and Br in the brightest internal regions, corresponding to encapsulated material, whereas I (from added surface functional groups) is distributed along the wall regions where carbon is present (individual SWNTs and bundles). Further evidence for surface functionalization was obtained by coupling/decoupling fluorenylmethoxycarbonyl (Fmoc) groups on the amine termini of the functional groups that had been added to the SWNTs; the Fmoc chromophore has a characteristic peak at 301 nm in the ultraviolet-visible absorption spectra, enabling it to be measured spectrophotometrically (Supplementary Fig. S6).

Encouraged by the successful functionalization of filled SWNTs preserving the encapsulated CuBr, we constructed SWNT-biomolecule conjugates as a strategy to reduce the reported cytotoxicity and water insolubility of pristine carbon nanotubes (CNTs) that have hampered their use in biological applications²⁶. Such surface modifications of CNTs by biomolecules have the potential to improve their biocompatibility, water dispersibility and alter immunogenicity¹. Carbohydrate-containing structures (glycoconjugates) were chosen because they are widely seen in nature and play essential roles in many biological processes

including cell signalling, tissue localization and modulation of immune response^{10,27,28}. f-CuBr@SWNTs were coupled with the sugar *N*-acetylglucosamine (GlcNAc) shown on branched (dendron, GlcNAc^D) structures, after cleavage of NBoc protecting groups, to afford biomolecule-functionalized, filled SWNTs, GlcNAc^D-CuBr@SWNTs (Fig. 1).

The surface glycosylation of SWNTs was confirmed by ³H tagging with β 1,4-galactosyltransferase (GalT) and fluorescent labelling (Supplementary Information²⁹). GalT specifically catalyses the transfer of galactose from UDP-galactose (UDP-Gal) to the C-4 hydroxyl group of terminal GlcNAc residues in GlcNAc^D-CuBr@SWNTs to form *N*-acetyllactosamine (LacNAc). After first confirming the activity of GalT towards GlcNAc dendrons, GlcNAc^D (Supplementary Information and Figs S11, S12), [³H]-labelled UDP-Gal was then coupled to the GlcNAc termini of GlcNAc^D-CuBr@SWNTs. Not only did these methods specifically confirm the presence of the sugar GlcNAc as the biomolecule found on GlcNAc^D-CuBr@SWNTs, but they demonstrated the ready alteration of the surface functional groups to introduce either alternative biomolecules (LacNAc), radiolabels (³H) or fluorophores (naphthalimide triazole).

Next we explored the potential of these readily functionalized and filled capsule-like entities *in vivo*, in particular to act as defined containers capable of localizing radionuclides. Iodide radioemitters used for treatment of thyroid cancer are considered to be among the most effective for systemic radiotherapy^{30,31}. This approach is successful but specific for this organ because a thyroid iodide transport protein increases thyroid iodide concentrations 20–40-fold above those found in plasma; their use in the treatment of other diseased sites therefore is not yet clinically advanced. Filled, functionalized SWNTs were created in which CuBr was replaced with Na¹²⁵I. The incorporation of NaI into SWNTs was first tested with non-radioactive NaI; Z-contrast STEM, high-resolution transmission electron microscopy and EDS analysis confirmed successful encapsulation (Supplementary Figs S16–S18). Next, SWNTs were filled with Na¹²⁵I (to create Na¹²⁵I@SWNTs), and were then functionalized using the same protocol as described for CuBr-filled SWNTs, namely 1,3-dipolar cycloaddition (resulting in f-Na¹²⁵I@SWNTs) followed by the attachment of GlcNAc^D (resulting in GlcNAc^D-Na¹²⁵I@SWNTs). The biodistribution of ¹²⁵I

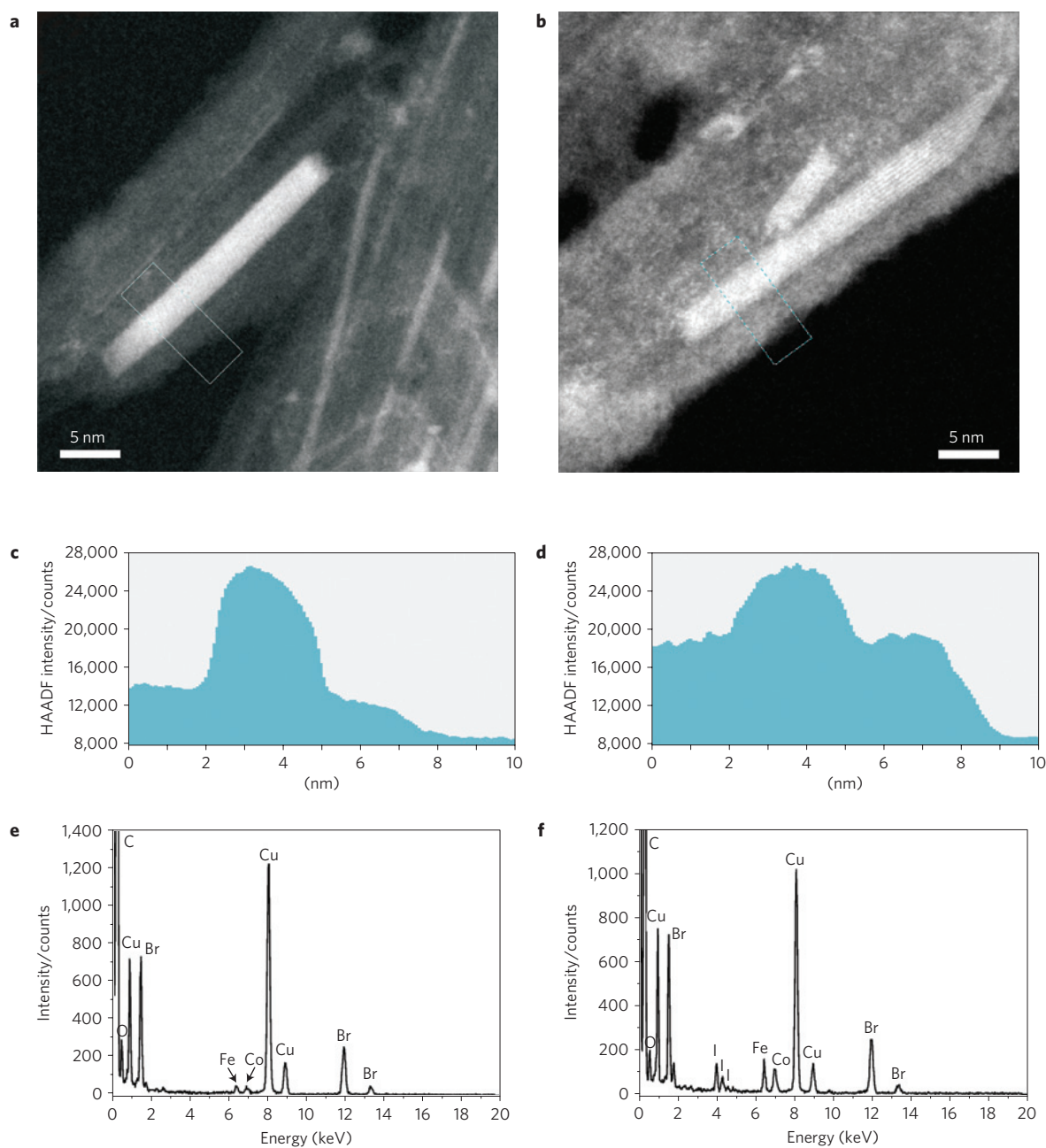


Figure 2 | Simultaneous detection of filling and functionalization. **a, b**, Z-contrast STEM images of CuBr@SWNTs (**a**) and f-CuBr@SWNTs (**b**). Iodine can be clearly seen along the SWNTs as well as CuBr filling inside SWNTs. For ease of comparison the bundles of SWNTs shown contain filled tubes of similar diameters and therefore comparable signal. **c, d**, Their respective intensity profiles along the white boxes in **a** and **b** demonstrate that the intensity in the bundle area is higher for the f-CuBr@SWNTs, in agreement with the presence of the iodine atoms in surface functional groups that have a substantial contribution ($Z = 53$) to the signal. **e, f**, EDS analysis confirms the presence of Cu and Br in both CuBr@SWNT (**e**) and f-CuBr@SWNT (**f**) samples. (Note that the Cu signal also has a contribution from secondary X-rays generated at the supporting Cu grid.) Peaks arising from the iodine present in the functional groups can also be found in the functionalized sample.

can be conveniently evaluated in a non-invasive manner through detection of gamma radiation, enabling direct imaging. Its decay half-life (59 days) valuably enables imaging over extended periods. Two groups of animals ($n = 4-6$) were injected in the tail vein with $50 \mu\text{g}$ and $250 \mu\text{g}$ of GlcNAc^D-Na¹²⁵I@SWNTs, which contained 0.2 MBq and 1.0 MBq of radioactivity respectively. Such doses of radioactivity (0.2–1.0 MBq) are considerably lower than those used in imaging studies of carbon nanotubes by single-photon emission computed tomography (SPECT) previously³² or the standard clinically used doses for the purpose of whole-body imaging *in vivo* using SPECT; ref. 33). The minimum detectable radioactivity

dose of non-encapsulated Na¹²⁵I injected into the control group ($n = 4-6$) was 1.8 MBq.

SPECT/CT imaging was carried out immediately after tail-vein injection of the GlcNAc^D-Na¹²⁵I@SWNTs (Fig. 3a, left panel) or Na¹²⁵I (Fig. 3a, right panel) and after 4 h, 24 h and 7 d. Free Na¹²⁵I (unencapsulated) rapidly accumulated in the thyroid and stomach as well as being excreted into the urine (see the high signal in the bladder), as has been previously described by others³⁴ (Fig. 3a, right panel). For GlcNAc^D-Na¹²⁵I@SWNTs, the tissue distribution profile indicated predominantly lung accumulation (Fig. 3a, left panel) with no signals detected in the thyroid, stomach

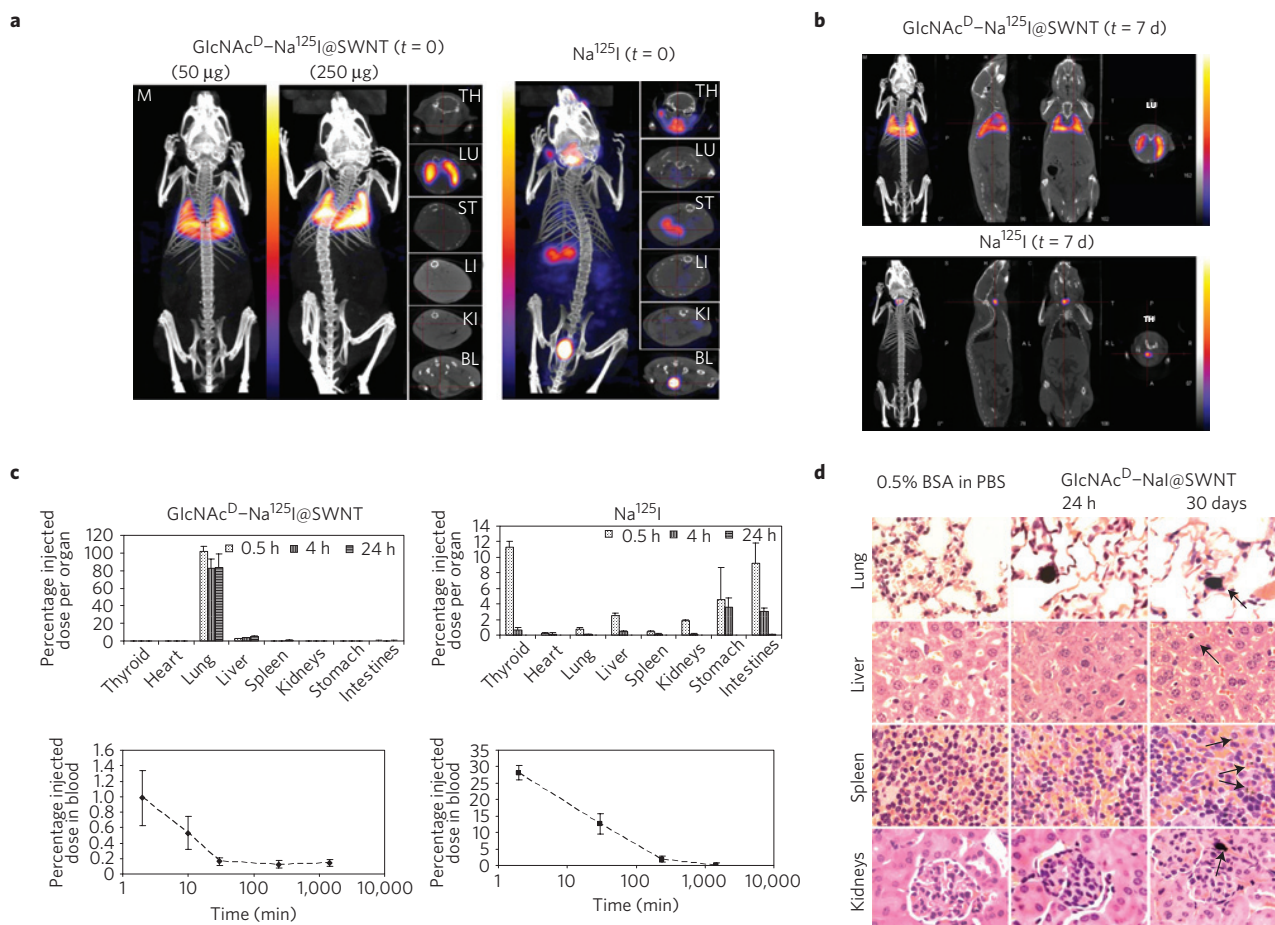


Figure 3 | Whole-animal SPECT/CT imaging, tissue biodistribution, blood circulation and histology following intravenous administration of filled, functionalized SWNTs. **a, b**, Whole-body SPECT/CT imaging was carried out immediately after tail-vein injection (**a**) and 7 days post-injection (**b**) of the $\text{GlcNAc}^{\text{D}}\text{-Na}^{125}\text{I}@\text{SWNT}$ s (50 μg and 250 μg ; 0.2 MBq and 1.0 MBq, left-hand side in **a** and upper panels in **b**) or Na^{125}I (1.8 MBq, right-hand side in **a** and lower panels in **b**) with a scanning time of 40–60 min. Cross-sections of the thyroid (TH), lung (LU), stomach (ST), liver (LI), kidney (KI) and bladder (BL) at equivalent time points are shown. **c**, Tissue biodistribution and blood-clearance profile of $\text{GlcNAc}^{\text{D}}\text{-Na}^{125}\text{I}@\text{SWNT}$ s (50 μg , 0.2 MBq, left-hand panels) or Na^{125}I (0.36 MBq, right-hand panels) in mice after tail-vein injection. The percentage injected dose per organ was calculated at 30 min, 4 h and 24 h after injection. Data are expressed as means \pm s.d. ($n = 4\text{--}6$). **d**, Haematoxylin- and eosin-stained sections of lung, liver, spleen and kidney at 24 h and 30 days post-administration with ‘cold’ $\text{GlcNAc}^{\text{D}}\text{-Na}@\text{SWNT}$ s (50 μg) or vehicle alone (0.5% BSA in PBS). Clearance to liver and kidney is consistent with SWNTs being slowly excreted through biliary and urinary routes (black arrows indicate nanotubes). All photomicrographs were captured at $\times 40$ magnification.

or bladder. Together, these data suggested that ^{125}I was stably encapsulated in $\text{GlcNAc}^{\text{D}}\text{-Na}^{125}\text{I}@\text{SWNT}$ s with no release of the radionuclide *in vivo* following administration. Consequently, the tissue distribution of this radioemitter had been dramatically altered compared with that of free Na^{125}I . Imaging at later time points (4 h and 24 h) showed persistent retention of the $\text{GlcNAc}^{\text{D}}\text{-Na}^{125}\text{I}@\text{SWNT}$ s into the lung (Supplementary Fig. S19a), whereas free Na^{125}I was mainly retained in the thyroid and stomach after 4 h and only in the thyroid after 24 h (Supplementary Fig. S19b). $\text{GlcNAc}^{\text{D}}\text{-Na}^{125}\text{I}@\text{SWNT}$ s showed persistent lung accumulation even after 7 days post-administration, in contrast to trace signals of the control, unencapsulated Na^{125}I that remained in the thyroid during the same period (Fig. 3b). These observations were considered as evidence of effectively complete encapsulation of radionuclide within the SWNT capsule and stability of the construct *in vivo* even after one week from administration.

Photon attenuation can compromise the accuracy of signal quantification using SPECT by up to 41% in the case of ^{125}I injected in mouse-sized phantom studies^{35,36}. We therefore carried out a further, more quantitative study to assess the organ biodistribution and blood-clearance profile of the nanotube constructs by direct gamma counting. Mice ($n = 4\text{--}6$) were injected with the lower

dose of $\text{GlcNAc}^{\text{D}}\text{-Na}^{125}\text{I}@\text{SWNT}$ s (50 μg , 0.2 MBq), because it was shown by SPECT/CT that the biodistribution profile was not dose dependent. Consistent with SPECT/CT data, gamma counting indicated overwhelming lung accumulation for the $\text{GlcNAc}^{\text{D}}\text{-Na}^{125}\text{I}@\text{SWNT}$ s for up to 24 h (Fig. 3c, top left). In contrast, free Na^{125}I (control) was cleared from the body within the first 24 h (Fig. 3c, top right). Negligible (<1% of total injected dose) $\text{GlcNAc}^{\text{D}}\text{-Na}^{125}\text{I}@\text{SWNT}$ s was detected in the blood 3 min after administration owing to rapid lung accumulation (Fig. 3c, bottom left), whereas 27% of the total injected dose of Na^{125}I was detected in the blood 3 min after injection, with complete clearance from circulation within the first 24 h after administration (Fig. 3c, bottom right). The percentage of injected dose per gram tissue (Supplementary Fig. S20) confirmed that more than 80% of ^{125}I persisted in the lung for 24 h only when inside SWNTs.

Histological examination of lungs, liver, spleen and kidneys was then carried out to investigate any signs of acute (24 h) or longer-term (30 days) histopathological abnormalities (for example, tissue fibrosis) following intravenous administration of $\text{GlcNAc}^{\text{D}}\text{-Na}^{125}\text{I}@\text{SWNT}$ s. These (Fig. 3d) further confirmed localization of $\text{GlcNAc}^{\text{D}}\text{-Na}^{125}\text{I}@\text{SWNT}$ s in the lung at 24 h post-administration. Furthermore, and in agreement with the

SPECT/CT and gamma counting data, no accumulation of SWNTs was observed in the liver, spleen and kidneys and no sign of tissue necrosis in the lungs or other organs was evident histologically. Tissue histology 30 days after administration indicated lack of necrosis or fibrosis of the lung, even after persistent presence of the GlcNAc^D-Na¹²⁵I@SWNTs. Some degree of re-distribution to the liver, spleen and kidneys (black arrows in Fig. 3d) indicated that the carbon nanotubes deposited in the lung may translocate with time to other organs, and were consistent with SWNTs being slowly excreted through biliary and urinary routes; however, further studies to evaluate the clearance kinetics of the injected material should be carried out before further clinical development can proceed. The interaction of GlcNAc^D-Na¹²⁵I@SWNTs with the pulmonary tissue was further studied by an *in vitro* cytotoxicity assay (LDH) using a human lung epithelial cell line (A549). No cytotoxic response from this cell line was obtained following interaction with the GlcNAc^D-Na¹²⁵I@SWNTs for 24 h at concentrations up to 125 µg ml⁻¹ (Supplementary Fig. S21). This striking localization and persistence of these novel biomolecule-functionalized constructs accompanied by apparently good tolerance (here in pulmonary tissue at least up to 30 days) is now under investigation for longer-term delivery of radionuclides. Lung-localized proteins known to bind the GlcNAc ligand, which we used here to functionalize the surface of GlcNAc^D-Na¹²⁵I@SWNTs, have been identified previously^{37,38}. The localization observed here may be due to specific engagement of these proteins by the surface ligands of GlcNAc^D-Na¹²⁵I@SWNTs or other physiological effects^{39,40}. Given the promising observations obtained in this study, further investigations to assess any longer-term toxicological and immunological responses to these long-residing SWNT constructs are warranted and are currently under development in our laboratories.

The absence of isotope leakage from the GlcNAc^D-Na¹²⁵I@SWNTs and the specific organ (lung) accumulation allowed for optimum target-to-background levels of detection and in this way ultrasensitive non-invasive imaging as well as precise localization of a highly concentrated 'radiodose'. Comparison of the level of concentrated radioemitter that may be delivered (Supplementary Information) by this nanoencapsulation method with previous systems that have used, for example, surface-chelated ⁶⁴Cu⁸ or ¹¹¹In⁵ or have explored optimized radiolabelled-antibody localization⁴¹ reveals a maximum potential radiodensity (> 5 × 10⁵ GBq/gCNT cf 10–70 GBq/gCNT) and radiodose (800–1,000% ID/g cf 10–20% ID/g; refs 5,8,41; Supplementary Fig. S20) that are, to our knowledge unprecedented. Such doses even greatly outstrip the dose localization achievable using ¹²⁵I alone in thyroid (70% ID/g in thyroid) on the basis of the very high natural affinity of that organ. Importantly, the 'leakage' of radiomaterials noted for other delivery systems⁴² is also entirely absent with the system described here. We speculate that modifications of the physicochemical properties of such nanocapsules and their surface functional groups may enable further control of their *in vivo* fate.

Methods

Na¹²⁵I@SWNTs: Molten phase filling of Na¹²⁵I. SWNTs were purified and shortened (majority of SWNTs <1 µm, major fraction 300 nm, as determined by atomic force microscopy) with steam at 900 °C (ref. 17) (Supplementary Information). SWNTs (1 mg), Na¹²⁵I (47 µl, 4.7 mCi, 1 × 10⁻⁵ M NaOH) and NaI (10 µl, 12 mg ml⁻¹) were transferred into a silica ampoule and heated to 70 °C overnight to remove water. The ampoule was sealed under vacuum and annealed at 900 °C for 4 h. The mixture was then washed with water to remove non-filled material, filtered and dried.

f-Na¹²⁵I@SWNTs: 1,3-dipolar cycloaddition on Na¹²⁵I@SWNTs. Na¹²⁵I@SWNT (1 mg), NBoc-amino acid 1 (1.0 mg, 3.3 µmol) and 2,3,5-triiodobenzaldehyde 2 (1.6 mg, 3.3 µmol) were dispersed in dimethyl formamide (dry, 2 ml) with sonication (1–2 min). The reaction mixture was refluxed at 120–130 °C for 96 h, cooled to room temperature and concentrated *in vacuo*. The residue was re-dispersed and washed with methanol. The sample was filtered on a polycarbonate

membrane (pore size: 0.2 µm) and dried *in vacuo*. Thin-layer chromatography (dichloromethane:methanol = 8:2) indicated the clear removal of reagents. Model reactions were conducted on C₆₀ (Supplementary Information).

GlcNAc^D-Na¹²⁵I@SWNTs: Glycosylation of f-Na¹²⁵I@SWNTs. f-Na¹²⁵I@SWNTs (1 mg) were dispersed in dichloromethane (dry, 2 ml) by sonication for 2 min. Trifluoroacetic acid (0.5 ml) was added to the suspension and the reaction mixture was stirred at room temperature for 1 h to afford amine termini by the cleavage of NBoc protecting groups. The mixture was concentrated *in vacuo* and dried under vacuum. Amine-terminated SWNTs were treated with GlcNAc^D (2 mg), *N,N*-diisopropylethylamine (1 µl) and *O*-(7-azabenzotriazol-1-yl)-*N,N,N'*,*N'*-tetramethyluronium hexafluorophosphate (1 mg) in dimethyl formamide (dry, 2.1 ml). The reaction mixture was sonicated for 2 min and stirred under Ar at room temperature. After 24 h, the reaction mixture was concentrated *in vacuo* and the residue re-dispersed, filtered, rinsed (methanol then water) and dried *in vacuo*. Thin-layer chromatography (water:isopropanol:ethyl acetate, 1:2:2) indicated the removal of reagents. A model study of GlcNAc^D-C₆₀ was characterized by one- and two-dimensional nuclear magnetic resonance, mass spectrometry and infrared spectroscopy (Supplementary Information and Figs S7–S9).

Preparation of GlcNAc^D-Na¹²⁵I@SWNTs aqueous dispersions.

GlcNAc^D-Na¹²⁵I@SWNTs were dispersed at a final concentration of 1 mg ml⁻¹ in 2.5% bovine serum albumin (BSA) (Sigma, UK) in DPBS (1.47 mM potassium phosphate monobasic, 2.66 mM potassium chloride, 137.93 mM sodium chloride, 8.06 mM sodium phosphate dibasic, Invitrogen, UK) by bath sonication for 45 min. Further dilutions of this stock were carried out using 5% dextrose for *in vitro* or DPBS for *in vivo* experiments.

Nano-SPECT/CT imaging of GlcNAc^D-Na¹²⁵I@SWNTs and Na¹²⁵I.

All experiments were conducted with previous approval from the UK Home Office. Balb/C mice were anaesthetized by isoflurane inhalation. Each animal was injected in the tail vein using 31G needles with 50 µg or 250 µg of GlcNAc^D-Na¹²⁵I@SWNTs containing approximately 0.2 MBq or 1.0 MBq, respectively. As a control, free Na¹²⁵I (1.8 MBq) was injected for comparison. All materials were injected in DPBS and in volume of 250 µl. Immediately after injection (*t* = 0) and at *t* = 4 h, *t* = 24 h and *t* = 7 d, mice were imaged using the nano-SPECT/CT scanner (Bioscan, USA). SPECT images were obtained in 16 projections over 40–60 min using a four-head scanner with 1.4 mm pinhole collimators. CT scans were taken at the end of each SPECT acquisition and all images were reconstructed with MEDISO software (Medical Imaging Systems). Fusion of SPECT and CT images was carried out using the PMOD software.

Tissue biodistribution of GlcNAc^D-Na¹²⁵I@SWNTs or Na¹²⁵I. Animals (*n* = 4–6) were injected with 250 µl containing 50 µg (0.2 MBq) of GlcNAc^D-Na¹²⁵I@SWNTs in 0.5% BSA or Na¹²⁵I (0.36 MBq) in 5% dextrose containing 0.2–0.5 MBq by tail-vein injection using 31 G needles. All materials were injected in DPBS. Blood was collected by bleeding 50 µl from the superficial tail vein at 3 min, 10 min, 30 min, 4 h and 24 h. Each animal was bled only twice during the whole experiment. At 30 min, 4 h and 24 h after injection, mice were killed and blood was collected. Thyroid, heart, lungs, liver, spleen, kidneys, stomach and intestines were sampled, each sample being weighed and counted on a gamma counter (Perkin Elmer, USA), together with a dilution of the injected dose with dead-time limit below 60%. The percentage injected dose per gram tissue or the percentage injected dose per organ was calculated for each tissue.

Histological examinations of GlcNAc^D-NaI@SWNTs were carried out at 24 h and 30 d post-injection (Supplementary Information).

Cell-viability assays of GlcNAc^D-NaI@SWNTs (7.8–125 µg ml⁻¹) against human pulmonary epithelial cells were carried out in triplicate after 24 h incubation at varying concentrations (Supplementary Information).

Received 2 October 2009; accepted 8 April 2010; published online 16 May 2010

References

- Weissleder, R. *et al.* Cell-specific targeting of nanoparticles by multivalent attachment of small molecules. *Nature Biotechnol.* **23**, 1418–1423 (2005).
- Martin, C. R. & Kohli, P. The emerging field of nanotube technology. *Nature Rev. Drug Disc.* **2**, 29–37 (2003).
- Wu, W. *et al.* Targeted delivery of Amphotericin B to cells by using functionalized carbon nanotubes. *Angew. Chem. Int. Ed.* **44**, 6358–6362 (2005).
- Prato, M., Kostarelos, K. & Bianco, A. Functionalized carbon nanotubes in drug design and discovery. *Acc. Chem. Res.* **41**, 60–68 (2008).
- Singh, R. *et al.* Tissue biodistribution and blood clearance rates of intravenously administered carbon nanotube radiotracer. *Proc. Natl Acad. Sci. USA* **103**, 3357–3362 (2006).
- McDevitt, M. R. *et al.* Tumor targeting with antibody-functionalized, radiolabeled carbon nanotubes. *J. Nucl. Med.* **48**, 1180–1189 (2007).

7. Hartman, K. B., Hamlin, D. K., Wilbur, D. S. & Wilson, L. J. ²¹¹AtCl@US-tube nanocapsules: A new concept in radiotherapeutic-agent design. *Small* **3**, 1496–1499 (2007).
8. Liu, Z. *et al.* *In vivo* biodistribution and highly efficient tumour targeting of carbon nanotubes in mice. *Nature Nanotech.* **2**, 47–52 (2007).
9. Meyer, R. R. *et al.* Discrete atom imaging of one-dimensional crystals formed within single-walled carbon nanotubes. *Science* **289**, 1324–1326 (2000).
10. Davis, B. G. Synthesis of glycoproteins. *Chem. Rev.* **102**, 579–601 (2002).
11. Liu, Z. *et al.* Imaging the dynamic behaviour of individual retinal chromophores confined inside carbon nanotubes. *Nature Nanotech.* **2**, 422–425 (2007).
12. Koshino, M. *et al.* Imaging of single organic molecules in motion. *Science* **316**, 853 (2007).
13. Iezzi, E. B. *et al.* Lutetium-based trimetallic nitride endohedral metallofullerenes: New contrast agents. *Nano Lett.* **2**, 1187–1190 (2002).
14. Koltover, V. K. in *Progress in Fullerene Research* (ed. Milton, L.) 199–233 (Nova, 2007).
15. Ohtsuki, T. *et al.* Insertion of Xe and Kr atoms into C₆₀ and C₇₀ fullerenes and the formation of dimers. *Phys. Rev. Lett.* **81**, 967–970 (1998).
16. Shao, L., Tobias, G., Huh, Y. & Green, M. L. H. Reversible filling of single walled carbon nanotubes opened by alkali hydroxides. *Carbon* **44**, 2855–2858 (2006).
17. Ballesteros, B. *et al.* Steam purification for the removal of graphitic shells coating catalytic particles and the shortening of single-walled carbon nanotubes. *Small* **4**, 1501–1506 (2008).
18. Chen, J. *et al.* Solution properties of single-walled carbon nanotubes. *Science* **282**, 95–98 (1998).
19. Chen, X. *et al.* Interfacing carbon nanotubes with living cells. *J. Am. Chem. Soc.* **128**, 6292–6293 (2006).
20. Wu, P. *et al.* Biocompatible carbon nanotubes generated by functionalization with glycodendrimers. *Angew. Chem. Int. Ed.* **47**, 5022–5025 (2008).
21. Chen, X. *et al.* Boron nitride nanotubes are noncytotoxic and can be functionalized for interaction with proteins and cells. *J. Am. Chem. Soc.* **131**, 890–891 (2009).
22. Tsang, S. C., Chen, Y. K., Harris, P. J. F. & Green, M. L. H. A simple chemical method of opening and filling carbon nanotubes. *Nature* **372**, 159–162 (1994).
23. Nellist, P. D. & Pennycook, S. J. Direct imaging of the atomic configuration of ultradispersed catalysts. *Science* **274**, 413–415 (1996).
24. Hong, S. Y. *et al.* Atomic-scale detection of organic molecules coupled to single-walled carbon nanotubes. *J. Am. Chem. Soc.* **129**, 10966–10967 (2007).
25. Ballesteros, B., Tobias, G., Ward, M. A. H. & Green, M. L. H. Quantitative assessment of the amount of material encapsulated in filled carbon nanotubes. *J. Phys. Chem. C* **113**, 2653–2656 (2009).
26. Kostarelos, K. The long and short of carbon nanotube toxicity. *Nature Biotechnol.* **26**, 774–776 (2008).
27. Dwek, R. A. Glycobiology: Toward understanding the function of sugars. *Chem. Rev.* **96**, 683–720 (1996).
28. Varki, A. Biological roles of oligosaccharides. *Glycobiology* **3**, 97–130 (1993).
29. Sawa, M. *et al.* Glycoproteomic probes for fluorescent imaging of fucosylated glycans *in vivo*. *Proc. Natl Acad. Sci. USA* **103**, 12371–12376 (2006).
30. Mazzaferri, E. L. in *The Thyroid: A Fundamental and Clinical Text* (eds Braverman, L. E. & Utiger, R. D.) 922–945 (Lippincott-Raven, 1996).
31. Spitzweg, C. *et al.* *In vivo* sodium iodide symporter gene therapy of prostate cancer. *Gene Therapy* **8**, 1524–1531 (2001).
32. Lacerda, L. *et al.* Dynamic imaging of functionalized multi-walled carbon nanotube systemic circulation and urinary excretion. *Adv. Mater.* **20**, 225–230 (2008).
33. Beekman, F. J. *et al.* Towards *in vivo* nuclear microscopy: Iodine-125 imaging in mice using micro-pinholes. *Eur. J. Nucl. Med. Mol. Imaging* **29**, 933–938 (2002).
34. Marsee, D. K. *et al.* Inhibition of heat shock protein 90, a novel RET/PTC1-associated protein, increases radioiodide accumulation in thyroid cells. *J. Biol. Chem.* **279**, 43990–43997 (2004).
35. Chen, C. L., Wang, Y., Lee, J. J. S. & Tsui, B. M. W. Toward quantitative small animal pinhole SPECT: Assessment of quantitation accuracy prior to image compensations. *Mol. Imaging. Biol.* **11**, 195–203 (2009).
36. Hwang, A. B., Franc, B. L., Gullberg, G. T. & Hasegawa, B. H. Assessment of the sources of error affecting the quantitative accuracy of SPECT imaging in small animals. *Phys. Med. Biol.* **53**, 2233–2252 (2008).
37. Kan, V. L. & Bennett, J. E. Lectin-like attachment sites on murine pulmonary alveolar macrophages bind *Aspergillus fumigatus* conidia. *J. Infect. Dis.* **158**, 407–414 (1988).
38. Hickling, T. P. *et al.* Collectins and their role in lung immunity. *J. Leukoc. Biol.* **75**, 27–33 (2004).
39. Kanke, M. *et al.* Clearance of ¹⁴¹Ce-labeled microspheres from blood and distribution in specific organs following intravenous and intraarterial administration in beagle dogs. *J. Pharm. Sci.* **69**, 755–762 (1980).
40. Illum, L. *et al.* Blood clearance and organ deposition of intravenously administered colloidal particles. The effects of particle size, nature and shape. *Int. J. Pharm.* **12**, 135–146 (1982).
41. Berndorff, D. *et al.* Radioimmunotherapy of solid tumors by targeting extra domain B fibronectin: Identification of the best-suited radioimmunoconjugate. *Clin. Cancer Res.* **11**, 7053s–7063s (2005).
42. Liu, Z. *et al.* Circulation and long-term fate of functionalized, biocompatible single-walled carbon nanotubes in mice probed by Raman spectroscopy. *Proc. Natl Acad. Sci. USA* **105**, 1410–1415 (2008).

Acknowledgements

We thank the Samsung Scholarship Foundation (S.Y.H.), the FP7 European Community Marie Curie ERG and Ramón y Cajal Programmes (G.T.), MICINN Spain (B.B.), INNS Japan (S.L.-P.) and Thomas Swan Co. Ltd. (SWNTs and funding), and K. Doores, O. Pearce, J. Errey, W. Liu and M. A. Ward for technical assistance. R.B.S. is a member of the European Community CARBIO research training network. K.K. and K.T.A.-J. would like to acknowledge partial funding of this work by the FP7 Anticarb (HEALTH-2007-201587) research programme. H.A.-B. wishes to acknowledge the Ministère de l'Enseignement Supérieur et de la Recherche Scientifique (Algeria) for a full Ph.D. scholarship. B.G.D. is a Royal Society–Wolfson Research Merit Award recipient and is supported by an EPSRC LSI platform grant.

Author contributions

S.Y.H., G.T., R.B.S., M.L.H.G., K.K. and B.G.D. designed the research, S.Y.H., G.T., K.T.A.-J., B.B., H.A.-B., S.L.-P., C.F. and S.J.M. carried out the experiments, S.Y.H., G.T., K.T.A.-J., H.A.-B., B.B., S.L.-P., P.D.N., R.B.S., S.J.M., M.L.H.G., K.K. and B.G.D. analysed the data and S.Y.H., G.T., K.T.A.-J., K.K. and B.G.D. wrote the paper.

Additional information

The authors declare no competing financial interests. Supplementary information accompanies this paper on www.nature.com/naturematerials. Reprints and permissions information is available online at <http://npg.nature.com/reprintsandpermissions>. Correspondence and requests for materials should be addressed to G.T., K.K. or B.G.D.